Pressure-induced volume collapse and structural phase transitions in SrRuO$_3$

Mikhail Zhernenkov [a,*,1], Gilberto Fabbris [a,b], Omar Chmaissem [c,d], J.F. Mitchell [d], H. Zheng [d], Daniel Haskel [a]

[a] Advanced Photon Source, Argonne National Laboratory, Argonne, IL 60439, USA
[b] Department of Physics, Washington University, St. Louis, MO 63130, USA
[c] Department of Physics, Northern Illinois University, DeKalb, IL 60115, USA
[d] Materials Science Division, Argonne National Laboratory, Argonne, IL 60439, USA

ABSTRACT

We report on the low temperature (6 K) structural properties of SrRuO$_3$ under quasi-hydrostatic pressure studied by synchrotron X-ray powder diffraction in a diamond anvil cell. First principle calculations predict a first-order perovskite (Pv) to post-perovskite (pPv) phase transition at ~40 GPa accompanied by a 1.9% volume collapse. Our results rule out the occurrence of a pPv phase to 54 GPa. Instead, we find a Pv to monoclinic to triclinic sequence of phase transitions. The monoclinic to triclinic phase transition at ~38 GPa is accompanied by a 3.5% volume collapse. X-ray absorption spectroscopy indicates that this volume collapse is not accompanied by a change in Ru valence state. Our results should help guide improvements to theoretical treatments of this and other correlated d-electron systems based on density functional theory.

Published by Elsevier Inc.

1. Introduction

During the past few decades, significant efforts have been devoted to the study of 3d transition metal oxides (TMOs), which are host to myriad phenomena of potential technological relevance such as high temperature superconductivity, colossal magneto-resistance, and multiferroicity [1–3]. The richness of phase diagrams that characterize these materials is tied to the ability to control the relative strength of on-site Coulomb interactions and electronic bandwidth in the quasi-localized 3d states. On the other hand, 4d orbitals of transition metals are more extended than their 3d counterparts, the quasi-delocalized states usually resulting in the absence of local moments or even itinerant magnetism [4]. SrRuO$_3$ stands out against other 4d TMOs as being the only ferromagnetic perovskite ABO$_3$ compound displaying a relatively high Curie temperature T_c~163 K [5]. It is a good electrical conductor, which is indicative of "band" or itinerant ferromagnetism of the 4d electrons. Due to its unique properties, SrRuO$_3$ is widely used as a metallic perovskite electrode in oxide based electronic and spintronic devices [6] and has been discussed as a candidate material to display exotic quantum critical phenomena, such as unconventional superconductivity and non-Fermi-liquid behavior [7,8]. The latter can be triggered by a small perturbation of the ground state; e.g., by the application of external hydrostatic pressure, magnetic fields or chemical doping [9].

According to recent theoretical calculations [10–12], SrRuO$_3$ was predicted to provide an example of the long sought-after perovskite to post-perovskite (Pv-to-pPv) phase transition under high pressure with a concomitant collapse of the ferromagnetic ground state. However, despite significant efforts neither the Pv-to-pPv phase transition nor the collapse of magnetism has been observed in SrRuO$_3$. Prior high-pressure studies reported that no structural transition occurs up to 34 GPa [13,14]. More recently, first-principles calculations based on density functional theory (DFT) predicted that SrRuO$_3$ will undergo a first order, ferromagnetic-Pv to non-magnetic pPv, phase transition with related volume collapse under hydrostatic pressure of about 40 GPa [15].

In this article we report a previously unknown structural transition in SrRuO$_3$ to triclinic P phase at ~38 GPa accompanied by a volume collapse of 3.5%. This transition is preceded by small monoclinic distortions of the initial Pv ($Pbnm$) phase within the pressure range of 21–38 GPa. The triclinic phase persists up to at least 54 GPa. While a volume collapse is indeed observed near 40 GPa as predicted by density functional theory [15], the lowest energy (experimental) structure is found to be triclinic instead of the predicted pPV structure [15].

* Corresponding author.
E-mail address: zherne@bnl.gov (M. Zhernenkov).
[1] Present address: Brookhaven National Laboratory, PO Box 5000, Upton, NY 11973, USA.

2. Experimental

2.1. Synthesis

Polycrystalline $SrRuO_3$ was prepared by solid-state reaction of stoichiometric ratios of $SrCO_3$ (99.994%) and RuO_2 (99.99%). The as-received severely hygroscopic RuO_2 powder was heated to 600 °C in a stream of nitrogen to remove water. The final product was made by firing in the following sequence: 900 °C/12 h in nitrogen, followed by subsequent firings in air at 700 °C, 750 °C, and 800 °C for 5 h each with intermediate grindings. Choice of the firing atmosphere was based on a detailed study of oxygen and Ru nonstoichiometry in $SrRuO_3$ published by Dabrowski et al. [16]. The reaction was deemed complete when no further change to the powder X-ray diffraction pattern was observed. DC magnetization revealed a sharp ferromagnetic transition at ~162 K, indicative of a high quality stoichiometric $SrRuO_3$ phase (see Fig. 1). $SrRuO_3$ has an orthorhombically distorted perovskite structure with *Pnma* space group (No. 62) at ambient pressure. Hereafter the non-standard space group *Pbnm* is used to be consistent with the published literature. Space group *Pnma* has a doubled *b* axis with respect to the cubic perovskite structure whereas *Pbnm* has a doubled *c* axis and the transformation from *Pnma* to *Pbnm* is obtained by $a_1 \rightarrow b_2$, $b_1 \rightarrow c_2$, and $c_1 \rightarrow a_2$.

2.2. High pressure XRD experiment

High-pressure X-ray diffraction (XRD) experiments were performed in a Mao-type symmetric diamond anvil cell (DAC) in combination with cubic boron nitride seats on a polycrystalline $SrRuO_3$ sample at HP-CAT beam line 16-BM-D of the Advanced Photon Source (APS), Argonne National Laboratory. In this study, two different pressure media, namely neon and helium, were used in order to discriminate against non-hydrostatic stress effects [17]. The powder $SrRuO_3$ sample was loaded in DACs with a full diamond anvil opposite a partially perforated diamond anvil with culet sizes of 300 μm (DAC loaded with neon) and 180 μm (DAC loaded with helium) together with small ruby spheres and gold powder for in-situ pressure calibration [18,19]. Rhenium gaskets 250 μm-thick were pre-indented to a thickness of about 1/6 of the culet size. Holes with a diameter of about 2/5 the culet size were

drilled in the center of the pre-indented region. Helium and Neon gases were loaded using the COMPRES/GSECARS gas-loading system at APS [20] at pressures of 2.5 GPa and 5 GPa, respectively. Samples in DACs with neon and helium were measured at two different wavelengths of $\lambda = 0.37713$ Å and 0.41646 Å, respectively. The powder XRD patterns were recorded using a MAR image plate camera with a 100×100 μm^2 pixel size with 10 min integration times for high signal-to-noise ratio. Fits to the data were achieved by Rietveld and/or LeBail methods, using the EXPGUI-GSAS system suite [21].

2.3. High pressure XANES experiment

In order to clarify the nature of the phase transitions and the volume collapse the high pressure diffraction data were supplemented by X-ray absorption near edge structure (XANES) measurements at the Ru K-edge (~22.1 keV). The high pressure XANES experiment was performed at the 4-ID-D beam line of the APS in a membrane driven copper–beryllium DAC with 300 μm diamonds. In order to avoid contamination of XANES spectra by Bragg peaks from the diamond anvils, a common occurrence at the high energy of the Ru K-edge, XANES measurements were performed in transmission geometry where the X-ray beam goes through a beryllium gasket. The gasket was initially pre-indented to 65 μm, and then the whole culet area drilled and replaced by BN powder, which was compressed so that at 20 GPa the thickness was 60 μm. This procedure was used to ensure that the gasket thickness would be larger than the beam size at the highest pressures. The sample, together with a ruby sphere and Si oil as a pressure medium, were all loaded in a sample chamber ~80 μm in diameter made at the center of the BN insert. A pair of Kirkpatrick–Baez (KB) mirrors was used to focus the beam to $~10 \times 10$ μm^2. Incident and transmitted beams were measured using a N_2 filled ion chamber and a Si photodiode, respectively.

3. Results and discussion

3.1. XRD data

The $SrRuO_3$ sample was initially measured at room temperature and low pressures (2.5 GPa with He, and 5 GPa with Ne pressure media, Fig. 1). The lattice parameters obtained from the Rietveld refinements at 2.5 GPa [$a = 5.5516(4)$ Å, $b = 5.5130(9)$ Å, $c = 7.8220(1)$ Å] and 5 GPa [$a = 5.5340(5)$ Å, $b = 5.4855(6)$ Å, $c = 7.7955(7)$ Å] for the orthorhombic *Pbnm* (No. 62) structure are in good agreement with the results of Hamlin et al. [13].

Subsequently, the DACs were cooled to a base temperature of 6 K and XRD patterns were collected at different pressures up to 54 GPa. Pressure was adjusted in-situ without removing the DACs from the cryostat and each pressure point was stabilized for about 15 min prior to data collection. XRD patterns collected at pressures from 10 GPa to 54 GPa are shown in Fig. 2 with expanded views of the data in the regions near the dashed lines shown in Figs. 3 and 4.

A full Rietveld refinement of the structure has been performed using data collected at 10 GPa. Data measured at 21 GPa and higher pressures were fit using the LeBail method [22] since typical Rietveld refinements are hampered by severe pressure-induced peak broadening and overlap. Fits using the the LeBail method yield information on the best possible space group symmetry and the corresponding lattice parameters but no useful information can be obtained for the fractional atomic coordinates.

Analysis of the diffraction data shows the expected systematic shift with pressure of the peaks to smaller *d*-spacing values. In addition, splitting of the diffraction peaks at 21 GPa indicates the occurrence of a structural change from orthorhombic *Pbnm*
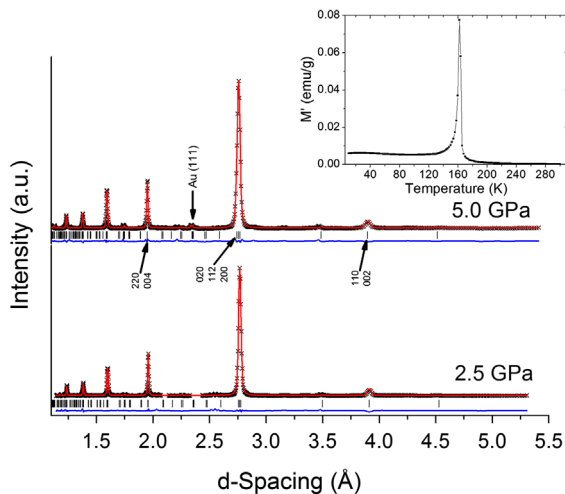

Fig. 1. XRD patterns from a polycrystalline $SrRuO_3$ sample measured at 300 K for two pressure values of 2.5 GPa (He pressure medium) and 5 GPa (Ne pressure medium). Best-fit Rietveld refinements are also shown (solid lines). For the 2.5 GPa pattern, two small excluded data regions between 2 Å and 2.5 Å correspond to the Re gasket diffraction peaks. The insert shows the derivative of the DC magnetization curve with a sharp ferromagnetic transition at ~162 K.

(No. 62) to a lower monoclinic symmetry of space group $P2_1/n$ (No. 14). The derivation of the space group symmetry is discussed below. In the orthorhombic *Pbnm* phase, a major peak group at d-spacing of $\sim$2.74 Å (10 GPa) actually consists of three peaks: (2 0 0) at 2.7467 Å, (1 1 2) at 2.7293 Å, and (0 2 0) at 2.7082 Å. In the monoclinic phase at 21 GPa, the (1 1 2) peak splits into two peaks (1 1 2 and 1 1 $\overline{2}$). The peaks are now positioned 1 1 2 as (1 1 $\overline{2}$) at 2.7307 Å, (1 1 2) at 2.700 Å, (0 2 0) at 2.6840 Å, and (2 0 0) at

2.6804 Å. Further at 23 GPa, the peak positions evolve to: (1 1 $\overline{2}$) at 2.7281 Å, (0 2 0) at 2.7015 Å, (1 1 2) at 2.6807 Å, and (2 0 0) at 2.6498 Å. The split 1 1 2 peaks (1 1 2 and 1 1 $\overline{2}$) are only consistent with a lower than orthorhombic symmetry; thus, giving firm evidence for the appearance of the monoclinic phase. In addition, a feeble splitting of (2 2 0) and (0 0 4) peaks (positioned at 1.9284 Å and 1.9314 Å, respectively) at 10 GPa in *Pbnm* phase dramatically enhances at pressures above 21 GPa (Fig. 3). For comparison, had the data at 21 GPa been fitted with the *Pbnm* symmetry, the resulting χ^2 – a measure of goodness of fit [23] – would deteriorate by about 57% and the prominent (2 2 0) and (0 0 4) peaks splitting could not be reproduced. Therefore, the data taken at 21 GPa cannot be described with the *Pbnm* structure. The monoclinic $P2_1/n$ phase with a monoclinic angle $90.9° < \beta < 91.5°$ persisted up to 36 GPa.

The observed orthorhombic to monoclinic phase transition is consistent with theoretical analysis carried out using the online software ISOTROPY developed by Campbell and Stokes [24]. The fact that no superstructure reflections appear under pressure implies that Γ must be the k-point vector to be investigated. All other k-points allowed by the symmetry of the parent *Pbnm* structure require the doubling or rotation of one or more unit cell parameters. With this in mind, the only possible continuous distortions can be accommodated by the orthorhombic *Pbnm*, $P2_12_12_1$, $Pmn2_1$, $Pmc2_1$, $Pna2_1$ and the monoclinic $P2_1/m$ and $P2_1/n$ (standard $P2_1/c$) space groups. However, since the split peaks cannot be indexed using any orthorhombic space groups we are only left with $P2_1/m$ and $P2_1/n$ space groups as possible solutions. The difference between these two solutions is mainly related to the distortion pattern of the oxygen atoms which cannot be resolved satisfactorily with X-rays. Nonetheless and despite the small X-ray scattering length of oxygen, best-fit LeBail refinements were obtained using the $P2_1/n$ symmetry as shown in Fig. 3. Additionally, we also note that both the *Pbnm* and $P2_1/n$ symmetries belong to the same $a^- a^- c^+$ octahedral tilt system as described by Woodward et al. and Glazer's notation [25–27] while $P2_1/m$ is not. We also note that the original Glazer tilt systems only considered the continuous distortions from cubic *Pm-3m* to pseudocubic superstructures of a similar unit cell size. Woodward and his coworkers [27] expanded this idea to include ordered superstructures or larger supercells similar to ours (with
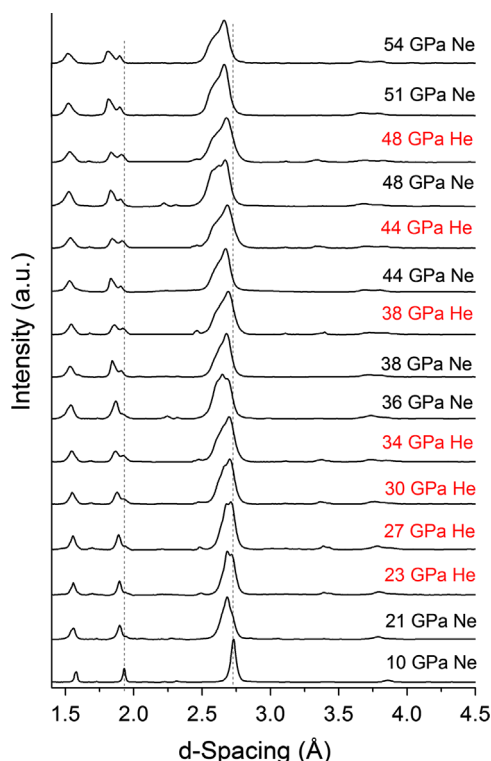

Fig. 2. XRD patterns measured at 6 K in the pressure range of 10–54 GPa with two different pressure media (He and Ne, indicated near each curve). Flat curve regions between 2.0 Å and 2.3 Å in the data measured with He correspond to the exclusions of Re gasket diffraction peaks. Dashed lines serve as guide to the eye highlighting the peaks shift.
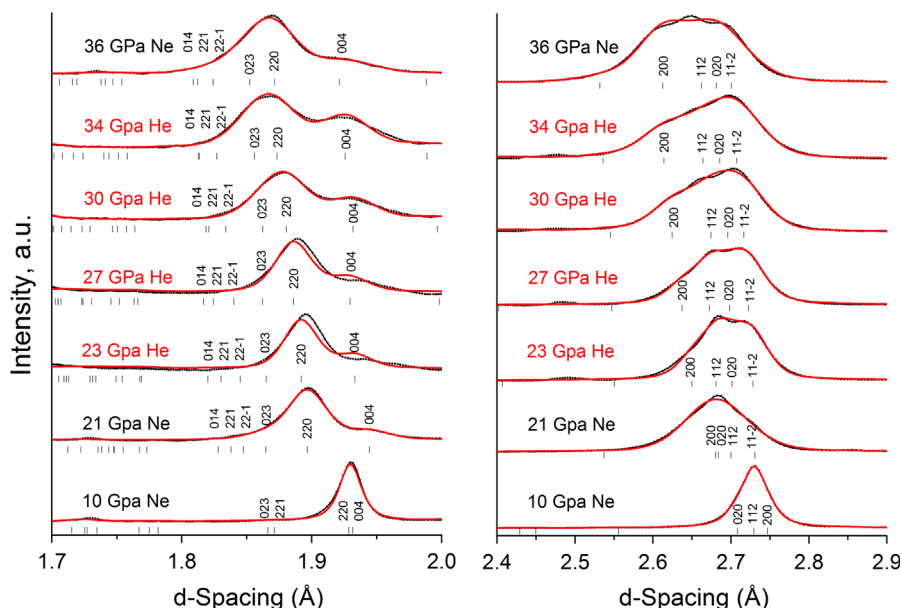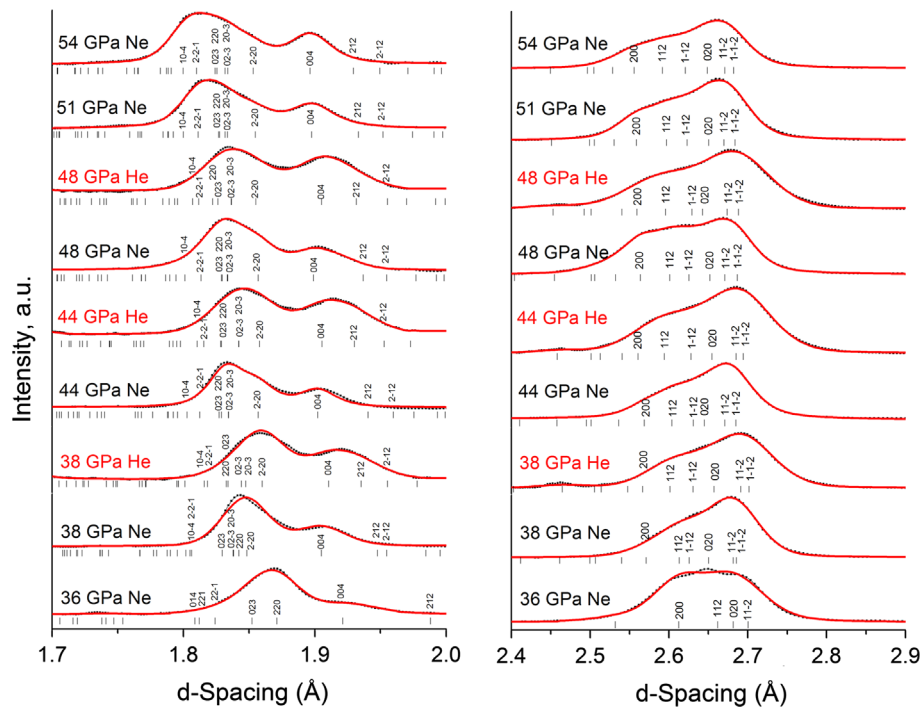

Fig. 3. Pressure-dependent XRD data for selected Bragg peaks measured with He and Ne pressure media for pressure range 10–36 GPa, together with their Rietveld (10 GPa) and Le Bail ($P > 10$ GPa) refinements.

Fig. 4. Pressure-dependent XRD data for selected Bragg peaks measured with He and Ne pressure media for pressure range 36–54 GPa, together with their Le Bail refinements.

Table 1
Lattice parameters and unit cell volume for SrRuO$_3$ as a function of pressure ($T=6$ K).

P (GPa)	a (Å)	b (Å)	c (Å)	α (°)	β (°)	γ (°)	V (Å)
10 (Ne)	5.4934(3)	5.4164(3)	7.7259(4)	90.00	90.00	90.00	229.885(11)
21 (Ne)	5.3615(27)	5.3680(10)	7.7778(25)	90.00	90.91(3)	90.00	223.82(18)
23 (He)	5.3012(7)	5.4031(6)	7.7350(12)	90.00	91.40(1)	90.00	221.489(34)
27 (He)	5.2761(6)	5.3964(6)	7.720(1)	90.00	91.49(1)	90.00	219.738(30)
30 (Ne)	5.2507(4)	5.3919(4)	7.7288(7)	90.00	91.25(1)	90.00	218.763(23)
34 (He)	5.2294(4)	5.3714(4)	7.7048(8)	90.00	91.29(1)	90.00	216.373(26)
36 (Ne)	5.2260(2)	5.3628(4)	7.687(2)	90.00	91.14(3)	90.00	215.398(49)
38 (Ne)	5.1450(8)	5.3005(7)	7.6245(8)	90.25(1)	91.93(1)	90.18(1)	207.813(35)
38.5 (He)	5.1383(8)	5.3151(9)	7.6498(10)	90.28(1)	92.41(1)	90.83(1)	208.714(20)
44 (Ne)	5.1406(4)	5.2904(4)	7.6129(6)	90.19(1)	91.83(1)	90.86(1)	206.912(16)
44.2 (He)	5.1266(5)	5.3101(8)	7.6287(9)	90.38(1)	92.36(1)	90.90(1)	207.470(17)
47.7 (He)	5.1227(9)	5.2862(8)	7.6258(9)	90.29(2)	92.07(1)	91.01(1)	206.340(32)
48 (Ne)	5.1308(4)	5.3042(4)	7.6011(6)	90.13(1)	91.97(1)	90.84(1)	206.726(41)
51 (Ne)	5.1212(3)	5.3016(3)	7.5955(4)	90.18(1)	92.01(1)	90.84(1)	206.076(13)
54 (Ne)	5.1160(6)	5.2982(8)	7.5913(9)	90.27(1)	92.12(1)	90.85(1)	205.606(71)

$a{\sim}b{\sim}\sqrt{2}a_p$ and $c{\sim}2a_p$ where a_p is the cubic perovskite unit cell dimension). There are many examples in the literature showing similar transitions taking place between the same two space groups (e.g., GdFeO$_3$ and similar ferrites [28], Y$_{1-x}$Ca$_x$TiO$_3$ [29], nickelates and manganites, etc. [30]).

A complete set of unit cell parameters, including angles and volume as a function of pressure is given in Table 1. The pressure-dependent volume data in Table 1 were fitted with a second-order Birch–Murnaghan (B–M) equation of state (EOS) [31] below 36 GPa (Fig. 5) since the limited number of data points and pressure range up to the volume collapse prevents us from accurately determining both the bulk modulus and its pressure derivative. The corresponding fitted curve (lower dashed line in Fig. 5) yielded values of $V_0=237(1)$ Å^3 for the unit cell volume at ambient pressure and $B_0=323(18)$ GPa for the bulk modulus. As expected, this bulk modulus measured at 6 K is larger than its value at 300 K ($B_0=192$ GPa; Ref. [13]). We also carried out a fit to the B–M equation including the ambient pressure data point measured by

neutron diffraction in Ref. [26] (241.5 Å^3 at $T=1.5$ K). The corresponding fit (upper dashed line in Fig. 5) yielded values of $V_0=240.1(1.5)$ Å^3 and $B_0=260(25)$ GPa for the bulk modulus. This last fit is consistent, within errors, with both the X-ray data and the ambient pressure neutron data [32]. Note that forcing a third-order B–M EOS with a pressure derivative of the bulk modulus $B_0'=5$ from Ref. [13] returns $B_0=246(22)$ GPa, which is within one to two standard deviations from the values obtained by the second order B–M EOS fits. We do not have enough knowledge of the exact cationic or anionic stoichiometry of the sample used in Ref. [32]. Hence, inclusion of the neutron results from Ref. [32] in our fits may not be fully warranted and an accurate determination of B_0 would become difficult to achieve. We note that our sample is inferred to be stoichiometric based on its sharp magnetic transition with 162 K ordering temperature, as reported in the systematic study of T_c vs. stoichiometry in SrRuO$_3$ [16]. Nevertheless, the main focus of this paper is not providing an exact measurement of the bulk modulus of SrRuO$_3$ but rather testing the theoretical
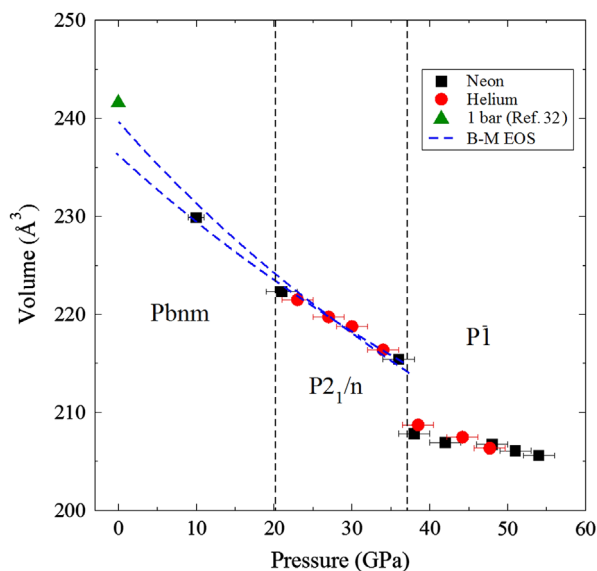
Fig. 5. Unit cell volume as a function of pressure ($T = 6$ K). Black squares and red circles correspond to Ne and He pressure media, respectively. Blue dashed lines are fit to the data before the volume collapse using a second-order *B–M* EOS excluding (lower curve) and including (upper curve) neutron diffraction data for the low temperature, ambient pressure volume. Dashed lines denote structural phase boundaries. The volume at ambient pressure ($T = 1.5$ K) is from Ref. [32]. Volume error bars are smaller than the symbol size. (For interpretation of the references to color in this figure legend, the reader is referred to the web version of this article.)

prediction of a pV to ppV structural phase transition accompanied by a volume collapse at around 40 GPa. While we clearly observe the latter, a pV to ppV transition does not take place.

Another signature of the structural transition into a monoclinic phase is the non-monotonic behavior of the lattice parameters in the 10–23 GPa pressure range (see Table 1). It is well known that most of the *Pbnm* GdFeO$_3$-type structures have lattice parameters $a < b < c$. However, in the case of SrRuO$_3$ this relation is not satisfied. SrRuO$_3$ is a compound for which $a > b$ at ambient conditions. Interestingly, in the monoclinic phase (at and above 21 GPa) the lattice parameters become consistent with the expected $a < b < c$ trend as with other GdFeO$_3$-type structures. At the same time, the pressure-dependent volume, $V(P)$, can still be explained with a *B–M* EOS. We note that a non-monotonic behavior of the lattice parameters has also been observed for SrRuO$_3$ within a similar pressure range, albeit at room temperature [13]. The previous study [13], reported $a > b$ up to 12.8 GPa, a sudden change to $a < b$ at 14.1 GPa, and a reversal back to the original trend at higher pressures to 25.3 GPa. Here we observe $a < b$ at and above 21 GPa where the monoclinic structure is observed. This apparent disagreement in the pressure dependence of lattice parameters may be a result of the different temperatures used in the experiments (6 K vs 300 K) or non-hydrostatic conditions related to the use of Si oil pressure transmitting medium in Ref [13]. A similar transformation from *Pbnm* to *P2$_1$/n* structure has been observed in *R*NiO$_3$ perovskites when the lattice is contracted by changing the rare-earth (*R*) ion type [33]. The small Ho^{3+} and Y^{3+} cations induce a monoclinic phase with inequivalent Ni sites displaying distorted NiO$_6$ octahedra [33]. The gradual increase of the structural distortion with reduction in *R* ionic size results in the structural transition to a monoclinic structure. Unfortunately, in the present study the relatively short range of XRD scattering angles ($< 25°$) limited by the design of the pressure cell, coupled with the inherently low X-ray scattering amplitude from oxygen atoms ($\sim Z$ atomic number), prevents the determination of the order parameter responsible for the RuO$_6$ octahedral distortions as a function of pressure.

As the pressure increases beyond 36 GPa, the XRD patterns (Fig. 2) can no longer be indexed using the *P2$_1$/n* monoclinic space group and the broadened peak shape profiles (Fig. 4) cannot be reproduced. Instead, using the LeBail fit procedure we observed a second phase transition to a lower P-type triclinic symmetry. The transition features a dramatic change in peak shape profiles especially at the *d*-space positions of ≈ 2.65 Å and ≈ 1.87 Å (Fig. 4), as seen by comparing the data measured at 36 GPa and 38 GPa with Ne pressure medium. For these two data sets, the LeBail fit revealed a concomitant volume collapse of 3.5%. The angles α and γ in the triclinic phase do not exceed 90.4° and 91°, respectively (Table 1). For comparison, had the data above 36 GPa been poorly fit with the *P2$_1$/n* structural model, the resulting χ^2 would have increased by a factor of 2.7 (54 GPa data), 9 (48 GPa data), and 16 (44 GPa data). Evidently, data taken above 36 GPa cannot be described by a monoclinic structure. Note, that the small diffraction peak around 2.25 Å in the 36 GPa and 48 GPa data (Ne data sets, Fig. 2) is the Au (1 1 1) peak from the Au pressure calibrant.

Theoretical analysis using ISOTROPY shows that continuous distortions from both the monoclinic *P2$_1$/m* or *P2$_1$/n* space groups can only lead to the triclinic *P$\bar{1}$* (No. 2) space group. The lower *P1* (No. 1) triclinic symmetry would have been possible if super-structures were to be observed or possibly with first-order structural transitions. While we can rule out the formation of superstructures, our data does indicate a first-order like phase transition and consequently *P1* (No. 1) cannot be excluded at this stage. Nonetheless, at these extreme pressures, to distinguish between *P1* from *P$\bar{1}$* would require the precise determination of all oxygen positions and therefore it cannot be reliably done. Neutron diffraction would be the ideal tool to determine the oxygen positions and the exact effects of pressure on the structure. However, such experiments would be extremely challenging because of the large pressures needed to drive the structural transitions with the related constraints on beam collimation and sample size. The best fit to our data using the *P$\bar{1}$* (No. 2) space group is shown in Fig. 4.

As noted in the introduction, previous DFT calculations [15] predicted a phase transition from Pv-SrRuO$_3$ to pPv-SrRuO$_3$ with a *Cmcm* crystal structure and a volume collapse of 1.9% at a pressure of 40 GPa. Instead, in the present study we observe a monoclinic to triclinic phase transition at similar pressures, but no signature of the pPv phase can be seen in the diffraction patterns. The comparison of the data measured at 38 GPa and the simulated theoretical pPV diffraction pattern for the predicted SrRuO$_3$ *Cmcm* crystal structure [15] at 40 GPa using the same Cagliotti parameters (GU, GV, GW, LX, LY [21]) are shown in Fig. 6. The absence of two major groups of diffraction peaks with *d*-spacing in the 2.1–2.3 Å and 2.8–3.0 Å range in the bottom panel of Fig. 6 clearly rules out the formation of a high-pressure, post-perovskite orthorhombic structure in SrRuO$_3$.

3.2. XANES data

Finally, Ru K-edge XANES measurements were performed at room temperature in order to probe for possible Ru valence changes that may take place at the high-pressure volume collapse transition. XANES provides element specific formal valence and information on the chemical and electronic structures including coordination environment (number and local symmetry). The sequence of XANES spectra measured at different pressures, together with their energy derivatives, is shown in Fig. 7. The spectra were normalized to a unit edge jump in order to account for possible variations in the sample thickness as the pressure increased. We found no evidence of a shift in the absorption edge of Ru as a function of applied pressure. This indicates that no
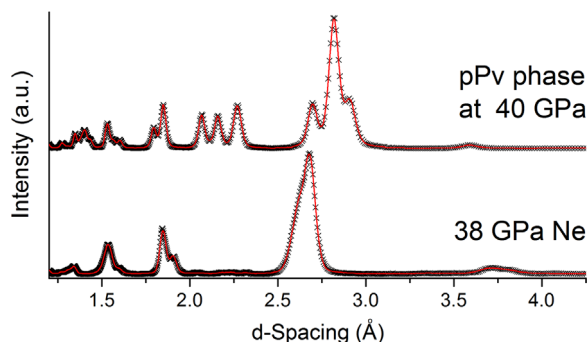
Fig. 6. (top) Simulated diffraction pattern from pPv-SrRuO$_3$ *Cmcm* crystal structure using atomic coordinates from Ref. [15]; (bottom) data measured in this study at 38 GPa with corresponding Le Bail fit.
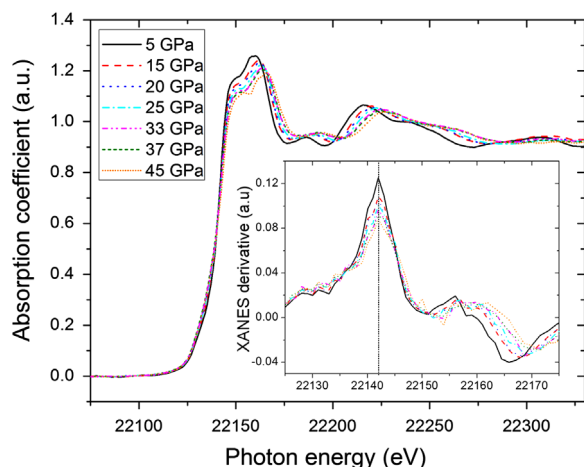

Fig. 7. Ru K-edge XANES spectra measured at different pressures using transmission geometry through a Be gasket. The inset is an expanded view of the energy derivative of the XANES spectra, showing the absence of any detectable Ru valence transition in this pressure range.

significant charge transfer or a change in Ru valence takes place across the full sequence of phase transitions. Furthermore, we conclude that the volume collapse is not electronically driven by a valence transition of the Ru ions.

4. Conclusions

In summary, we probed both the crystal structure and electronic structure of SrRuO$_3$ under high pressures up to 54 GPa. We observed a previously unpredicted sequence of structural phase transitions, namely perovskite orthorhombic *Pbnm* to monoclinic *P*2$_1$/*n* between 10 GPa and 21 GPa to triclinic *P* at ~38 GPa. The latter transition is accompanied by a volume collapse of 3.5%. The observed phase transitions are sequenced according to the maximal non-isomorphic subgroups classification and they are in agreement with group theoretical analysis performed using ISO-TROPY. We do not observe the theoretically predicted [15] perovskite to post-perovskite phase transition at 40 GPa. XANES measurements confirm that the Ru valence is unaffected by the applied pressures and rule out such a change as being responsible for the volume collapse during the phase transition. Our results provide important guidance and impose strong restrictions on future theoretical calculations aimed at understanding the structural and electronic ground states of SrRuO$_3$ and related complex oxides under high hydrostatic pressures.

References

[1] N.F. Mott, Metal-Insulator Transitions, Taylor & Francis, London/Philadelphia, 1990.
[2] P. Fazekas, Lecture Notes on Electron Correlation and Magnetism, World Scientific, Singapore, 1999.
[3] M. Imada, A. Fujimori, Y. Tokura, Rev. Mod. Phys. 70 (1998) 1039–1263.
[4] James S. Schilling, High pressure in science and technology, in: C. Homan, R. K. Mac Crone, and E. Whalley (Eds.), MRS Symposia Proceedings No. 22 North Holland, NY, 1984, p. 79.
[5] A. Callaghan, C.W. Moeller, R. Ward, Inorg. Chem. 5 (1966) 1572–1576.
[6] C.B. Eom, R.J. Cava, R.M. Fleming, Julia M. Phillips, R.B. vanDover, J.H. Marshall, J.W.P. Hsu, J.J. Krajewski, W.F. Peck Jr., Science 258 (1992) 1766–1769.
[7] L. Capogna, A.P. Mackenzie, R.S. Perry, S.A. Grigera, L.M. Galvin, P. Raychaudhuri, A. J. Schofield, C.S. Alexander, G. Cao, S.R. Julian, Y. Maeno, Phys. Rev. Lett. 88 (2002) 076602.
[8] P. Kostic, Y. Okada, N.C. Collins, Z. Schlesinger, J.W. Reiner, L. Klein, A. Kapitulnik, T.H. Geballe, M.R. Beasley, Phys. Rev. Lett. 81 (1998) 2498–2501.
[9] G.G. Lonzarich, Nat. Phys. 1 (2005) 11–12;
C. Pfleiderer, Rev. Mod. Phys. 81 (2009) 1551–1624;
Y. Matsumoto, S. Nakatsuji, K. Kuga, Y. Karaki, N. Horie, Y. Shimura, T. Sakakibara, A.H. Nevidomskyy, P. Coleman, Science 331 (2011) 316–319;
M. Dzero, M.R. Norman, I. Paul, C. Pepin, J. Schmalian, Phys. Rev. Lett. 97 (2006) 185701.
[10] K. Hirose, Rev. Geophys 44 (2006) RG3001.
[11] S. Tateno, K. Hirose, N. Sata, Y. Ohishi, Phys. Chem. Miner. 32 (2006) 721–725.
[12] H. Kojitani, Y. Shirako, M. Akaogi, Phys. Earth Planet. Inter 165 (2007) 127–134.
[13] J.J. Hamlin, S. Deemyad, J.S. Schilling, M.K. Jacobsen, R.S. Kumar, A.L. Cornelius, G. Cao, J.J. Neumeier, Phys. Rev. B: Condens. Matter 76 (2007) 014432.
[14] M.K. Jacobsen, R.S. Kumar, G. Cao, J.J. Neumeier, A.L. Cornelius, J. Phys. Chem. Solids 69 (2008) 2237–2239.
[15] Yongmao Cai, Yingjin Wei, Xing Ming, Fei Du, Xing Meng, Chunzhong Wang, Gang Chen, Solid State Comm 151 (2011) 798–801.
[16] B. Dabrowski, S. Kolesnik, O. Chmaissem, T. Maxwell, J. Mais, J.D. Jorgensen, Phys. Status Solidi 243 (2006) 13–20.
[17] K. Takemura, J. Appl. Phys. 89 (2001) 662–668.
[18] J.C. Chervin, B. Canny, M. Mancinelli, High Press. Res 21 (2001) 305–314.
[19] Yingwei Fei, Angele Ricolleau, Mark Frank, Kenji Mibe, Guoyin Shen, Vitali Prakapenka, PNAS 104 (2007) 9182–9186.
[20] Mark Riversa, Vitali B. Prakapenka, Atsushi Kubo, Clayton Pullins, Christopher M. Holl, Steven D. Jacobsen, High Press. Res 28 (2008) 273–292.
[21] B.H. Toby, J. Appl. Cryst. 34 (2001) 210–213;
A. C. Larson, R.B. Von Dreele, Los Alamos National Laboratory Report LAUR 86-748 2004.
[22] A. Le Bail, H. Duroy, J.L. Fourquet, Mater. Res. Bull. 23 (1998) 447–452.
[23] Mikhail Zhernenkov, M.R. Fitzsimmons, Jerzy Chlistunoff, Jaroslaw Majewski, Ioan Tudosa, E.E. Fullerton, Phys. Rev. B: Condens. Matter 82 (2010) 024420.
[24] B.J. Campbell, H.T. Stokes, D.E. Tanner, D.M. Hatch, J. Appl. Cryst. 39 (2006) 607–614.
[25] P.M. Woodward, Acta Cryst., B 53 (1997) 32–43.
[26] A.M. Glazer, Acta Cryst., B 28 (1972) 3384–3392.
[27] P.W. Barnes, M.W. Lufaso, P.M. Woodward, Acta Cryst., B 62 (2006) 384–396.
[28] R. Cheruku, L. Vijayan, G Govindaraj, Current Microscopy Contributions to Advances in Science and Technology, in: A. Mendez-Vilas (Ed.), Formatex Research Center, 2012, p. 1312. (and references therein).
[29] K. Kato, E. Nishibori, M. Takata, M. Sakata, T. Nakano, K. Uchihira, M. Tsubota, F. Iga, T. Takabatake, J. Phys. Soc. Jpn. 71 (2002) 2082–2085.
[30] Haifeng Li, Synthesis of CMR Manganites and Ordering Phenomena in Complex Transition Metal Oxides, Forschungszentrum Julich Gmbh, Julich, 2008.
[31] F. Birch, J. Geophys. Res. 83 (1978) 1257–1268.
[32] S.N. Bushmeleva, V.Yu. Pomjakushin, E.V. Pomjakushina, D.V. Sheptyakov, A.M. Balagurov, J. Magn. Magn. Mat 305 (2006) 491–496.
[33] Jose A. Alonso, Maria J. Martinez-Lope, Maria T. Casais, Miguel A.G. Aranda, Maria T. Fernandez-Diaz, J. Am. Chem. Soc. 121 (1999) 4754–4762.